Proceedings of GT2005
ASME Turbo Expo 2005: Power for Land, Sea and Air
June 6-9, 2005, Reno-Tahoe, Nevada, USA

GT2005-68608

AN ENTROPY LOSS APPROACH FOR A MEANLINE BLADEROW MODEL WITH COUPLING TO TEST DATA AND 3D CFD RESULTS

John A. Reed
The University of Toledo
2801 W. Bancroft St.
Toledo, Ohio, 43606, USA
jreed@eng.utoledo.edu

Mark G. Turner
University of Cincinnati
PO Box 210070
Cincinnati, OH 45221-0070, USA
mark.turner@uc.edu

ABSTRACT

A methodology which couples a computational fluid dynamics simulation and a 1D meanline bladerow model employing entropy-based loss terms is presented. A 3D APNASA CFD flow solution of the GE90-94B was used to provide input to the 1D bladerow model, which computed entropy-generation terms from the flow state. These terms accounted for losses in mixing of leakage and cooling flow, and gross aerodynamics using bladerow entropy loss coefficients as defined by Denton. A description of the 1D model is presented. The 1D bladerow model was implemented in the NPSS system making it possible to easily construct *N*-stage component simulations. The 1D model was used to generate partial performance maps of the HPT and LPT for use in a coupled 0D-3D simulation of the full GE90 engine. To validate the approach, a data match of the GE EEE HPT at the design point has been made and presented. An extrapolation of the model to off-design points has compared favorably to the experimental data.

INTRODUCTION

In the past decade, considerable progress has been made in the design of highly efficient turbomachinery components. Efficiency, the summed value of the individual losses over the entire flow domain, is often used as a design parameter because it provides a simple way to evaluate the quality of a design. While efficiency is useful for this reason, designers can produce better designs if they can identify the losses at discrete locations in the flow domain. In standard design practice, losses are typically categorized as mechanical, profile, secondary shock and tip leakage losses. Physically, these losses are intertwined, and it is impossible to separate them. For convenience, empirical loss-correlations are used to generate loss-coefficients which are used in the design process despite the fact that they may not be physically based. Entropy-generation is a thermodynamic parameter which defines the irreversibilities due to non-ideal energy transfer. An analysis based on entropy-generation to calculate the losses is superior to that using loss-

NOMENCLATURE

m	mass flow rate
F	force
P	static pressure
P_o	stagnation pressure
q	heat flow
R	radius
s	specific entropy
T	static temperature
T_o	stagnation temperature
T_q	blade row torque
V	velocity
Z	distance along axis
α	absolute flow angle measured from the axial direction
β	relative flow angle measured from the axial direction
ζ_s	entropy loss coefficient
θ	circumferential direction
ϕ	radial flow angle
ω	angular velocity

Subscripts

1	at inlet to blade row or stage
2	at exit from blade row or stage
aero	aerodynamic loss process
c	coolant flow
des	design point conditions
h	hub
o	stagnation conditions
m	moving
mix	loss process due to mixing
s	stationary
surr	surroundings
t	tip

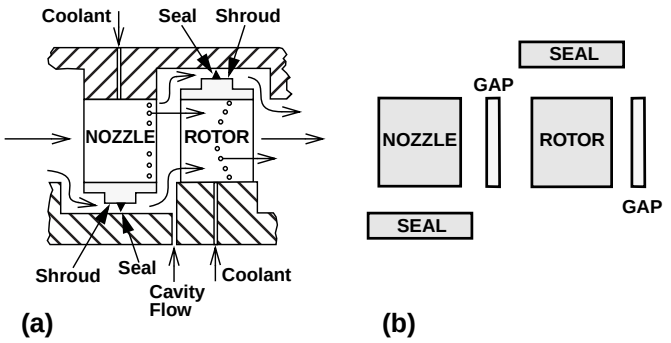

Figure 1. (a) Cross-section view of simplified shrouded turbine stage; (b) Control domains for turbine stage Nozzle, Gap, Seal and Rotor components.

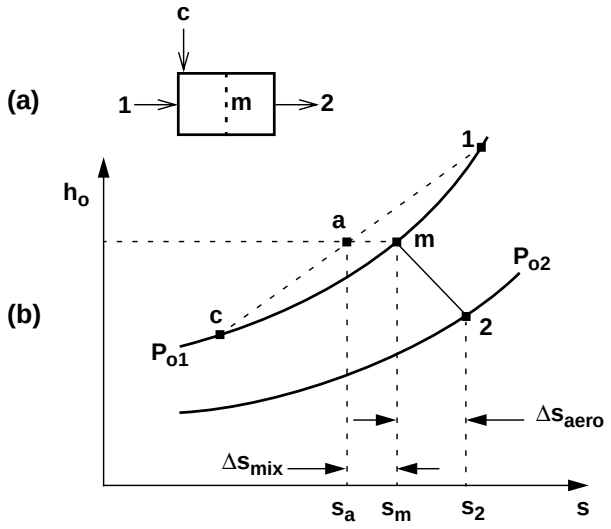

Figure 2. Mixing of two perfect gas flows at constant stagnation pressure.

correlations [1] as it can be computed at individual locations in the flow path.

The focus of this present effort is the development of a 1D meanline bladerow model employing entropy-based loss terms. The model is used as part of a larger simulation in which a cycle model of the GE90-94B high-bypass turbofan engine is coupled to a high-fidelity, full-engine model represented by a set of coupled 3D computational fluid dynamic (CFD) component models [2, 3]. Operating characteristics of the 3D component models are integrated into the cycle model via partial performance maps generated from the CFD flow solutions using the 1D bladerow model. These are actually "mini-maps" in the sense that they are developed only for a narrow operating range of the component.

Both the 1D and cycle model simulations utilize the Numerical Propulsion System Simulation (NPSS) thermodynamic cycle modeling system [4, 5]. This allows many features of the 1D model to be entirely consistent with the 0D or cycle, including the thermodynamics and cooling flows.

This paper describes the 1D bladerow model used to simulate the GE90-94B high-pressure turbine (HPT) and low-pressure turbine (LPT). The mathematical models for a shrouded turbine (the un-shrouded turbine uses the same model with no *Seal* Elements) and techniques for computing entropy due to mixing of leakage and coolant flows with the mainstream are developed using a control volume approach. The model is compared with test data for the GE Energy Efficient Engine (EEE) HPT. A methodology for generating 1D models of the HPT and LPT from a 3D CFD simulation is described. Finally, the partial turbine performance maps (mini-maps), generated by simulating each model over a small operating range around the GE90-94B take-off point, are presented.

METHODOLOGY

Consider the simplified model of Fig. 1a, which represents a shrouded turbine stage. The stage is fed by the main flow from the preceding stage or component. Leakage flow passes around the shroud and through the seal at the rotor tip and nozzle hub clearance. Coolant flow, bled from the compressor, is added to the mainstream through nozzle and rotor cooling holes, and expanded with it through the remaining stages of the turbine. Additional compressor flow, used to cool the disk cavity, enters the mainstream through the slot in the hub separating the nozzle and rotor. Control domains representing the primary stage elements, including the gap between bladerows, are shown in Fig. 1b.

An entropy-balance analysis on the control domain shown in Fig. 2a yields the following expression for entropy change for a 1D system:

$$m_2 s_2 = m_1 s_1 + m_c s_c + \frac{\dot{q}_{1\to 2}}{T_{surr}} + m_2 \Delta s_{tot} \qquad (1)$$

Entropy creation for fluid dynamic processes is due to *i*) viscous friction (e.g., mixing processes or a leakage jet), *ii*) heat transfer across finite temperature differences, and *iii*) non-equilibrium processes (e.g., shocks) [1]. Some or all of these processes may be present in the control domain at any one time, and identification of the individual sources is difficult. In order to simplify the analysis, we defined the total change in entropy as the sum of entropy changes due to: *i*) mixing two streams at different enthalpies, and *ii*) gross aerodynamic processes:

$$\Delta s_{tot} = \Delta s_{mix} + \Delta s_{aero} \qquad (2)$$

Entropy change due to mixing of the coolant and main flows having the same stagnation pressure but different stagnation temperatures is illustrated in Fig. 2b. The mass-averaged mixing of the two flows is identified by point *a*, located on the line between *1* and *c*. If mixing is assumed to occur at constant stagnation pressure, the actual mixed-out point will be *m*, which lies on the P_{o1} curve. Hence, the increase in entropy from *a* to *m* is due to the mixing process. This component of mixing loss is only due to the process illustrated in Fig. 2b. Other losses associated with mixing, such as a momentum loss, are included

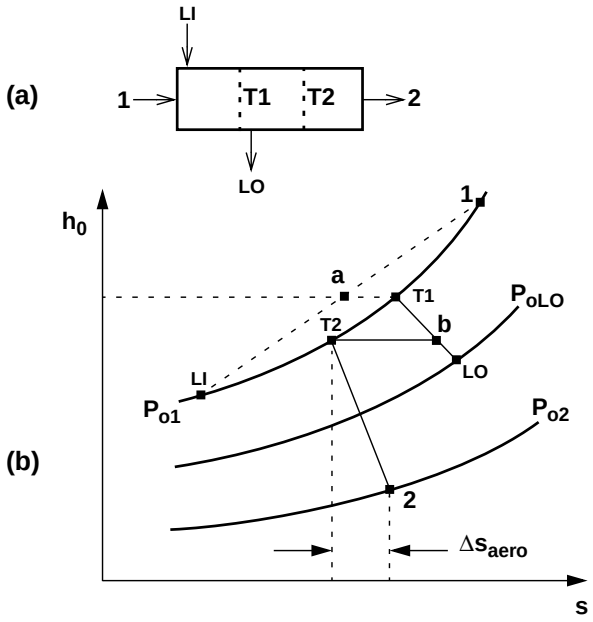

Figure 3. Addition and removal of leakage flows at constant stagnation pressure in Gap element.

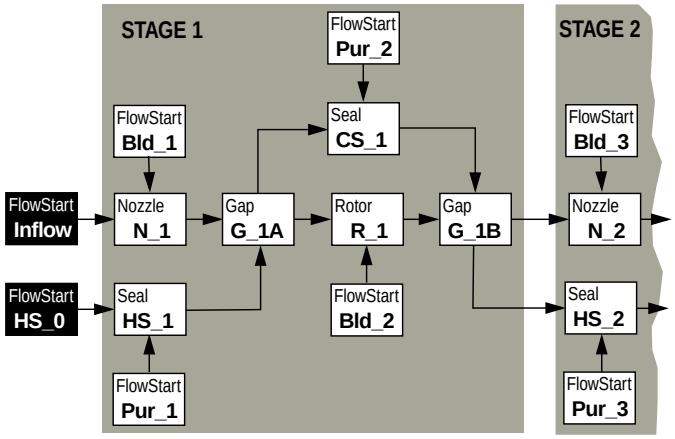

Figure 4. Partial turbine model schematic showing NPSS Nozzle, Rotor, Gap, Seal and FlowStart Elements.

in the Δs_{aero} term. The change in entropy between points *m* and *2* is due to the remaining loss mechanisms and is defined in terms of Denton's entropy loss coefficient [1]:

$$\zeta_s = \frac{T_2 \Delta s_{aero}}{h_{o2} - h_2} = \frac{T_2 \Delta s_{aero}}{0.5 V_2^2} \quad \text{for turbine blade rows} \qquad (3)$$

The entropy loss coefficient defined by Eq. (3) is used as a measurement of entropy generation in both stationary and rotating bladerows: nozzle and gap specific enthalpy terms are based on absolute velocities, while rotor specific enthalpy terms are based on relative velocities.

Applying conservation of mass to the control domain of Fig. 2a gives:

$$m_2 = m_1 + m_c \qquad (4)$$

Similarly, the energy balance can be expressed as

$$m_2 h_{o2} = m_1 h_{o1} + m_c h_{oc} + \omega(rF_\theta) + \dot{q}_{1\to 2} \qquad (5)$$

and angular momentum by

$$m_2 (rV_\theta)_2 = m_1 (rV_\theta)_1 + m_c (rV_\theta)_c + rF_\theta \qquad (6)$$

Equations (5) and (6) are consistent with the discussion by Lyman [6] on the conservation of energy and angular momentum including the torque and power terms in these equations.

Blade Row Gap Model

The axial gap between bladerows is a region of complex, unsteady flow due to rotor-nozzle interaction, as well as the addition and removal of leakage flows. For the nozzle-rotor gap, leakage flow enters and exits the gap from the nozzle hub seal and rotor tip seal, respectively. Similarly, in the rotor-nozzle gap, leakage flow enters the gap from the rotor tip seal and exits from the nozzle hub seal. In our simplified gap model, we assumed that leakage-in (LI) flow is first added to the mainstream at the same stagnation pressure, and mixes-out completely upon reaching station T1 (see Fig. 3a). Leakage-out (LO) flow is then removed from the mainstream prior to station T2, and the mainstream exits the gap at station 2.

Entropy changes due to flow addition, removal and mixing are illustrated in Fig. 3b. As described above, the mass-averaged flow state, point *a*, is located on the straight line between *1* and *LI*. Assuming constant stagnation pressure mixing, the actual flow state is defined at point *T1*. Leakage-out flow exits the gap at stagnation pressure P_{oLO}. Point *b*, on the line between *T1* and *LO* is determined by the leakage-out mass fraction. However, assuming constant-pressure mixing, the state of the flow at station *T2* will actually lie on the P_{o1} curve. The final change in flow state from *T2* to *2* is due to aerodynamic entropy production, Δs_{aero}, as defined in Eq. (3).

Shrouded Seal Model

Leakage flows were represented in the APNASA CFD model by flow sources and sinks. At the design point, seal exit mass flow rate and stagnation temperature were known from the CFD data; (rV_θ) was assumed to be $0.5\omega r^2$, which is the average of the stationary and moving boundary (rV_θ) values. At off-design operation, $(rV_\theta)_2$ was determined from the seal angular momentum equation:

$$m_2 (rV_\theta)_2 = m_1 (rV_\theta)_1 + m_c (rV_\theta)_c + (rF_\theta)_s + (rF_\theta)_m \qquad (7)$$

The $(rF_\theta)_s$ and $(rF_\theta)_m$ terms are the torque on the seal control domain due to the stationary and moving boundaries,

Table 1: Model input data.

Model Input Data	
Nozzle 1 inlet T_o (^oR)	1280.95
Nozzle 1 inlet P_o (psia)	50.163
Nozzle 1 inlet W (lbm/sec) (RDG 10)	24.015
Nozzle 1 exit hub radius (in.)	12.825
Nozzle 1 exit tip radius (in.)	14.400
Rotor 1 exit hub radius (in.)	12.730
Rotor 1 exit tip radius (in.)	14.410
Nozzle 2 exit hub radius (in.)	12.290
Nozzle 2 exit tip radius (in.)	14.980
Nozzle 2 exit hub radius (in.)	12.250
Nozzle 2 exit tip radius (in.)	15.000

respectively. At off-design, the torque was assumed to be given by

$$(rF_\theta) = (rF_\theta)_{des}\left[\frac{\omega}{\omega_{des}}\right] \tag{8}$$

The design-point stationary torque was then determined from the seal energy equation

$$m_2 h_{o2} = m_1 h_{o1} + m_c h_{oc} + \omega(rF_\theta)_m + \dot{q}_{1\to 2} \tag{9}$$

and used in Eq. (7) to solve for $(rF_\theta)_s$.

NPSS 1D Turbine Stage Model

NPSS *Element* classes corresponding to the nozzle, rotor, gap and seal components shown in Fig. 1 were written in the NPSS programming language. Each class declares attribute variables representing quantities appropriate for a given component, and solves the proper mathematical model described above. Additionally, a *FlowStart* class was written representing a flow source, and allowing its state (i.e., stagnation specific enthalpy, mass flow rate, etc.) to be specified. Instances of the *FlowStart* class are used to define bleed flow into the *Nozzle* and *Rotor*, and cavity purge flow into *Seal* elements. The schematic diagram of Fig. 4 illustrates how instances of these classes are combined to represent a turbine stage; the arrowed lines represent *links* which connect and exchange data between the NPSS elements. The `Inflow` and `HS_O` elements symbolize the main and leakage flows into the turbine first stage. Additional stages can be defined and connected to build a turbine model having any number of stages.

The use of the NPSS programming language is not a requirement of the proposed model. NPSS did offer several advantages including a thermodynamics package consistent with the cycle, robust solver tools, and the ability to eventually use this model within the cycle as a nested model.

Table 2: Model flow design data.

Design Parameter	Model	Design
N1 inlet absolute flow angle	0.0	0.0
N1 inlet absolute Mach No.	0.109	0.109
N1 exit absolute Flow angle	74.2	74.2
N1 exit absolute Mach No.	0.872	0.878
R1 exit relative Flow angle	65.8	66.9
R1 exit relative Mach No.	0.794	0.819
Stage exit absolute flow angle	12.2	17.7
Stage exit absolute Mach No.	0.334	0.338
N2 exit absolute Flow angle	68.6	69.0
N2 exit absolute Mach No.	0.764	0.828
R2 exit relative Flow angle	60.4	58.8
R2 exit relative Mach No.	0.839	0.836
Stage exit absolute flow angle	0.0	0.0
Stage exit absolute Mach No.	0.398	0.421

MODEL VALIDATION

The data used in the simulation of the GE90-94B is proprietary and cannot be disclosed. In order to demonstrate the validity of the 1D turbine simulation methodology, a model of the GE Energy Efficient Engine (EEE) HPT was developed. The Energy Efficient Engine program was the predecessor of the GE90 and the engines share similar features, making it a reasonable choice for a test case.

Data for the EEE model were obtained from GE test and design reports. EEE HTP model flow angles, Mach numbers, and flowpath geometry (see Tables 1 and 2) were based on final design values at the integrated core/low spool (ICLS) maximum climb cycle point listed in the hardware design report [7]. Inlet and cooling flow conditions (see Tables 1 and 4) were then defined based on reading (RDG) 10, from the results of the full-scale warm-air rig test [Appendix G, ref. 8]. Reading 10 represents a test point very near the ICLS design point.

All conditions at RDG 10 were matched in the model (see column 1, Table 5) by adjusting the entropy loss coefficients in each bladerow, Nozzle 2 exit angle, and both rotor exit angles. The loss coefficients (see Table 3) vary from 0.092 to 0.123. The other column in this table is the ratio of the change of entropy due to mixing to the change of entropy due to the aerodynamic

Table 3: EEE HPT entropy loss coefficients.

Element	ζ_s	$\Delta s_{mix}/\Delta s_{aero}$
Nozzle 1	0.0916718919204	1.19018
Rotor 1	0.0974222891114	0.76361
Nozzle 2	0.101726653726	0.14728
Rotor 2	0.122578757352	0.20853

Table 4: RDG 10 coolant flows.

Model Coolant Location	W_c (lbm/sec)	$P_{o,c}$ (psia)	$T_{o,c}$ (˚R)	Coolant Circuit
Nozzle 1 Aft Vane	1.14936	50.0749	629.647	Nozzle 1 Outer
Gap 1A Casing	0.128881			
Nozzle 1 Fwd Vane	0.849162	51.0625	586.256	Nozzle 1 Inner
Gap 1A Hub	0.302624	40.0012	592.917	CDP
Rotor 1	1.3320	49.6262	619.715	Inducer
Rotor 2	0.3068			
Gap 2B Hub	0.0605			
Gap 1B Hub	0.04064	23.472	641.632	Nozzle 2 Outer
Nozzle 2 Casing	0.50127			
Gap 2B Casing	0.03522			

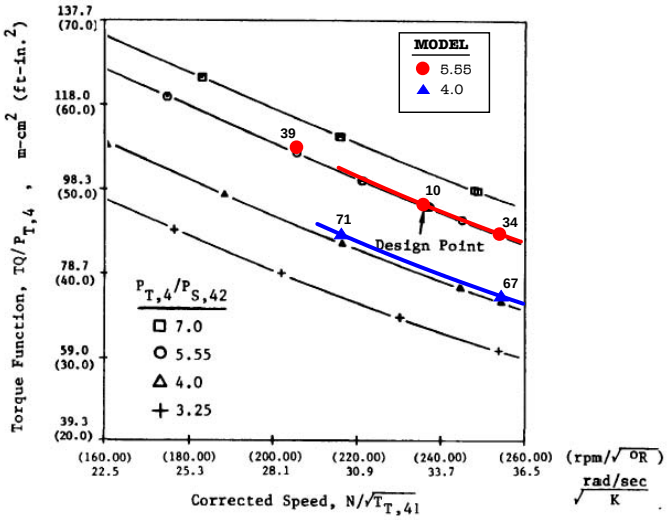

Figure 5. Comparison of measured and predicted torque function for the EEE HPT (overlaid on Fig. 60 from [8]).

loss. For nozzle 1 with a large amount of cooling flow, the mixing loss is larger by roughly 20%. For rotor 1, there is less cooling flow, and the mixing loss is roughly three-quarters of the aerodynamic loss. For the second stage with much less cooling flow, this ratio is then small.

The EEE HPT model was also run for four additional test readings. Coolant flows were set based on rig test data while the entropy loss coefficients were frozen at RDG 10 values. These four points represent off-design operating points on the total-to-static pressure ratio curves of 4.0 and 5.55. These results are tabulated in Table 5 and plotted in Figs. 5, 6, and 7. Model results (predicted) are overlaid on Figs. 60, 53 and 62 from the EEE HPT test report, respectively Also shown on these plots are extrapolations of the RDG 10 and RDG 71 models with a variation of the wheel speed. The total-to-static pressure ratios were maintained along with the coolant flows for these two readings.

The EEE HTP model captures the change of torque with pressure ratio and corrected speed as shown in Fig. 5. At the total-to-static pressure ratio of 4.0, where the model has been extrapolated, the predicted torque is slightly high. This is because the model is too efficient relative to the data. This is also seen in Fig. 6, comparing thermodynamic efficiency for a

Table 5: Comparison of measured and predicted flow data for five test-rig readings (RDG).

	RDG 10		RDG 34		RDG 39		RDG 67		RDG 71	
	Model	Rig	Model	Rig	Model	Rig	Model	Rig	Model	Rig
$P_{o,4}/P_{42}$	5.59431	5.59431	5.55603	5.55603	5.57590	5.5759	4.01443	4.01443	4.01867	4.01867
$P_{o,4}/P_{o,42}$	5.01834	5.01834	4.97996	4.97211	4.97075	4.97396	3.66947	3.63000	3.75676	3.73875
η_{TH}	0.8854	0.8854	0.8863	0.8862	0.8808	0.8736	0.88240	0.8664	0.8822	0.8664
Torque Function	48.2803	48.2804	44.6568	44.7349	55.0674	54.3161	37.3342	36.666	44.7609	43.5883
Flow Function	18.1967	18.1969	18.1579	18.1425	18.2629	18.2485	18.1155	18.0893	18.2131	18.1602
Blade-Jet Speed Ratio	0.57668	0.57666	0.62182	0.62201	0.50275	0.50254	0.67694	0.67824	0.57522	0.57612
Corrected Speed, N_c	235.968	235.966	254.047	254.049	205.567	205.568	254.477	254.482	216.306	216.316
Nozzle 1 exit P	29.3251	29.3250	29.8629	29.6704	27.8868	28.7199	30.2893	30.0974	29.1096	29.5377
Rotor 1 exit P	20.1112	20.1111	20.1909	20.1292	19.8019	20.0558	21.1001	20.9194	21.0741	20.9759
[a]Nozzle 2 exit P	14.1803	12.9287	14.1978	12.9554	14.1013	12.8599	15.9094	14.8638	16.0292	14.9148
Rotor 2 exit P	8.88479	8.88196	8.95742	8.92700	8.91748	8.95200	12.4207	12.3921	12.4330	12.4227

a. Test-rig values are hub sensor reading only.

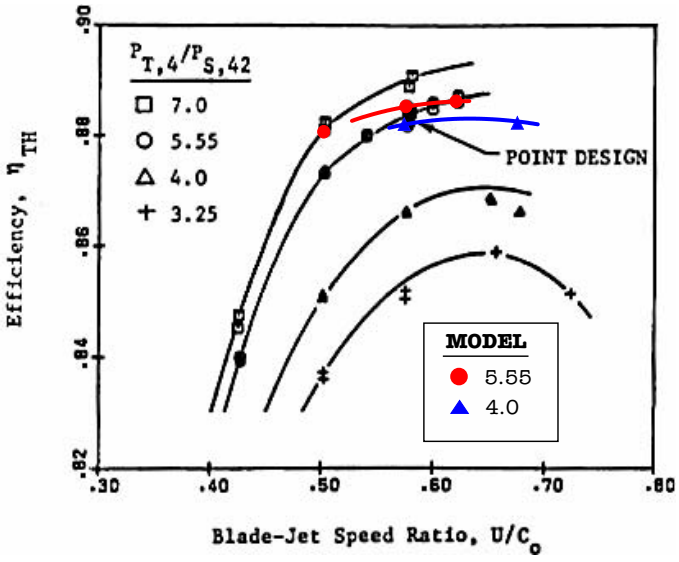

Figure 6. Comparison of measured and predicted thermodynamic efficiency for EEE HPT (overlaid on Fig. 53 from [8]).

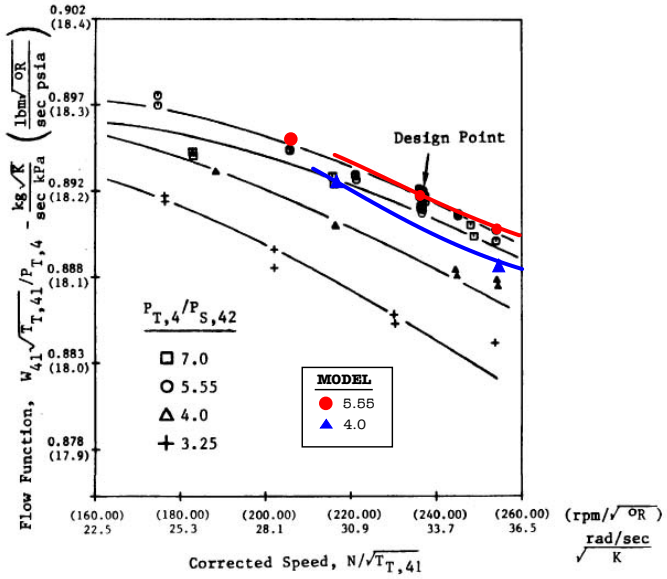

Figure 7. Comparison of measured and predicted flow function for EEE HPT (overlaid on Fig. 62 from [8]).

given blade-jet speed ratio. The trends are correct: the efficiency drops off for the lower pressure ratio, although the magnitude of the drop-off is considerably under predicted.This suggests that the entropy loss coefficient should not be held constant, or that additional individual loss mechanisms should be part of the loss model.

The flow function is plotted in Fig. 7. There is actually an inflection in the model for the 4.0 total-to-static pressure ratio. It is not yet understood why this is there, but can also be seen in the test data at the same pressure ratio. The drop-off in flow trend at the lower pressure ratio is captured, but the extent is not.

It should be emphasized that the 1D turbine model is valid for only a narrow region around the selected operating point (due to the assumption of constant entropy loss coefficient). The example shown has a speed range greater than +/- 10%, and the total-to-static pressure ratios went from 5.55 to 4.0, which are much larger than the mini-map extents that would have been used.

COUPLING TO 3D CFD RESULTS

NPSS 1D turbine models of the GE90-94B HPT and LPT were created in the semi-automated process shown in Fig. 8. Data from a converged APNASA 3D CFD simulation were first post-processed by the APNASA Circumferential Averaging Tool (APNASACAT), which read the 3D solution for each blade row, and performed circumferential area and mass averages of pressure, total pressure, total temperature, and other quantities of interest. The resulting data contained turbine flow quantities (m, T_o, P_o, h_o, α or β, ϕ, R_t, R_h and rV_θ) at the leading and trailing edges of each nozzle and rotor. These data, along with data specifying hub and tip seal leakage mass flow rates and stagnation temperatures, were then used as input to the *PreProcessorGenerator* program.

When executed, the *PreProcessorGenerator* parses the two input files, extracts the necessary data, and generates an intermediate data file and a connection file. The intermediate data file contains leading and trailing edge data for the *Nozzle*, *Rotor*, *Gap* and *Seal* elements in each of the turbine stages. The connection file describes the topology of the 1D turbine model in the form of NPSS *link* commands. The intermediate file was then used as input to the *TurbinePreProcessor* program.

The *TurbinePreProcessor* is responsible for translating the intermediate data file into an NPSS model. In addition, the data is used to compute: *i*) the entropy loss coefficient for each *Nozzle*, *Rotor* and *Gap*; *ii*) the enthalpy, pressure and mass fraction scalars for leakage-out flow in each *Gap*; *iii*) design torque values for each *Seal*, and *iv*) the correct mass flow rates in each element based on mass conservation (see discussion below on non-conserved quantities in CFD data). The *TurbinePreProcessor* outputs a temporary file which was then concatenated with the connection file to assemble the complete NPSS model.

For the GE90-94B, a two-stage high-pressure turbine (HPT) comprising 4 bladerows, and a six-stage low-pressure turbine (LPT) consisting of 12 bladerows, were constructed in this fashion. Although the LPT is un-cooled, *FlowStart* bleed elements (`Bld_1`, `Bld_2`, ...) were required in the model; thus, the mass flow rates were set to zero. Similarly, there were no tip leakage flows, so the mass flow rates from the disk cavities (defined by `Pur_2`, ...) into the tip *Seal* elements were set to zero. At the turbine exit (not shown), an instance of the *FlowEnd* class acts as a flow sink to terminate the flow.

Dealing With Non-conserved Quantities In CFD Data.

Variations in the averaged APNASA solution's mass flow rate, specific stagnation enthalpy and (rV_θ) were automatically

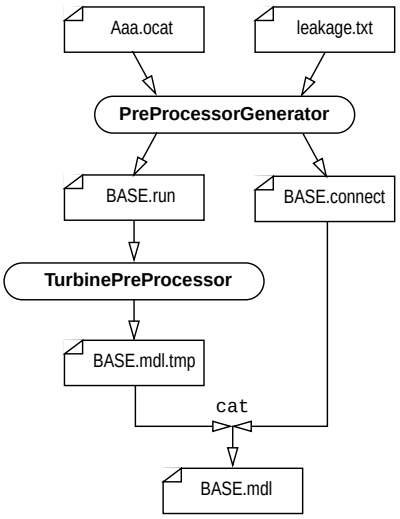

Figure 8. Process chart for generating NPSS 1D turbine model.

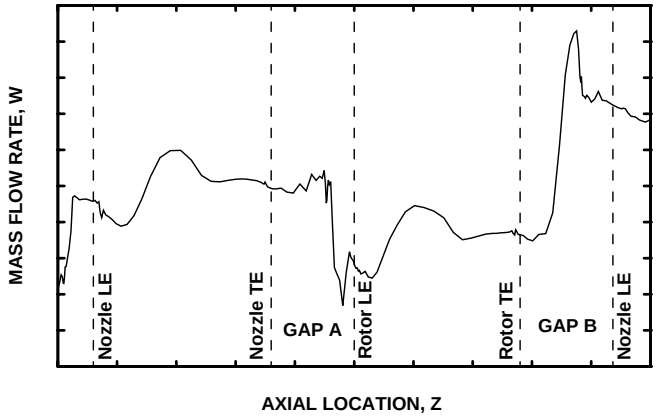

Figure 9. Variation of converged APNASA mass flow rate as a function of axial location for a single LPT stage. Nozzle and rotor leading and trailing edges (LE, TE) are indicated by vertical dashed lines.

adjusted by the *TurbinePreProcessor* to satisfy mass, energy and angular momentum conservation laws (Eqs. 4, 5, and 6). The CFD solution used here was the same one presented in refs. [2, 3]. It had been run for 10,000 iterations to demonstrate the full engine simulation. Any one blade row had mass conservation better than 0.4%. The simulation could have been converged further, but there will always be some variation in these parameters due to the approximate nature of the CFD method. This is illustrated in Fig. 9, which shows the fluctuation in mass flow rate across a single LPT stage with no nozzle or rotor cooling. The mass flow rate at the nozzle leading and trailing edges are clearly different, as is the mass flow rate at the rotor leading and trailing edges.

Adjusted mass flow rate values were computed by assuming the averaged APNASA turbine inlet, leakage and cooling mass flow rates were "correct", then applying the conservation of mass equation to get the leading-edge (LE) and trailing-edge (TE) mass flow rates for the remaining *Rotor*, *Nozzle* and *Gap* elements (differences in *Seal* inlet and exit mass flow rates were assumed to be purge flow). Variation in energy and angular momentum were handled slightly differently: averaged APNASA stagnation specific enthalpy and (rV_θ) at the exits of the *Nozzle* and *Rotor* were assumed "correct". Specific enthalpy and (rV_θ) at the intermediate locations were then computed from the energy and angular momentum conservation equations, respectively.

RESULTS

An APNASA simulation of the combined GE90-94B HPT and LPT (see Fig. 10), previously performed by Turner *et al.* [9], was used as input for the 1D model generation. The solution represents a sea-level, Mach 0.25, take-off condition. The main reason for this selection was that cooling flows for the turbine represent a significant amount of boundary condition information for the simulation, and these are best known at take-off. This condition also represents the heat transfer design point with the highest temperatures and most stress in the engine, and is thus an important condition to simulate.

The converged APNASA solution was post-processed by APNASACAT for both the HPT and LPT domains, and each were subsequently processed according to the procedure described in the methodology section. Adjusted mass flow rate, specific stagnation enthalpy, and (rV_θ) parameters at each bladerow leading and trailing edge were automatically computed by the *TurbinePreProcessor.*

A comparison of the converged APNASA and adjusted LPT mass flow rates is presented in Fig. 11. Across the LPT's 12 bladerows, the agreement between APNASA and 1D adjusted mass flow rate was adequate, with a maximum divergence of less than 1% occurring at the LPT exit. Comparison of the converged APNASA and adjusted LPT specific stagnation

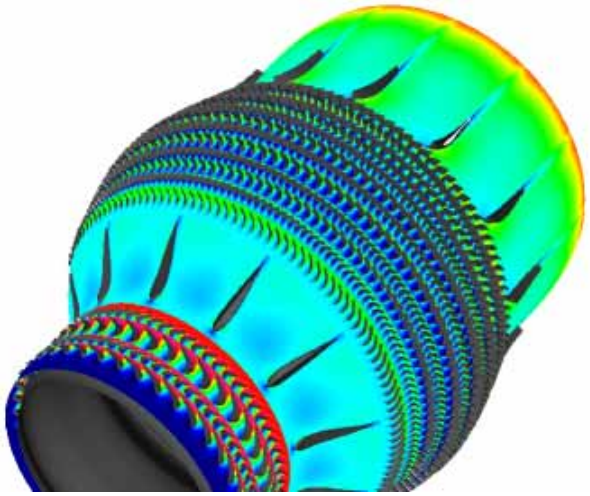

Figure 10. APNASA simulation of the combined GE90-94B HPT and LPT.

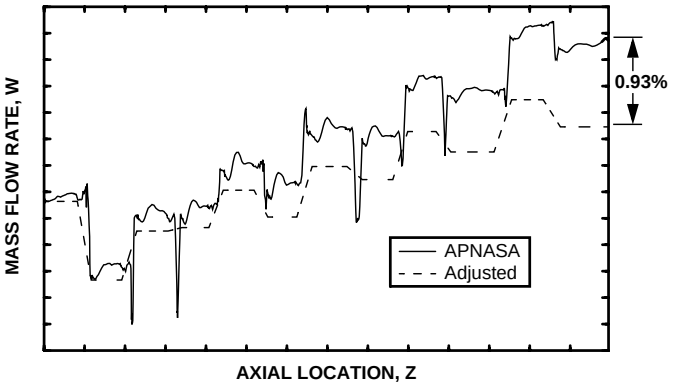

Figure 11. Comparison of converged APNASA and Adjusted LPT mass flow rate as a function of axial location.

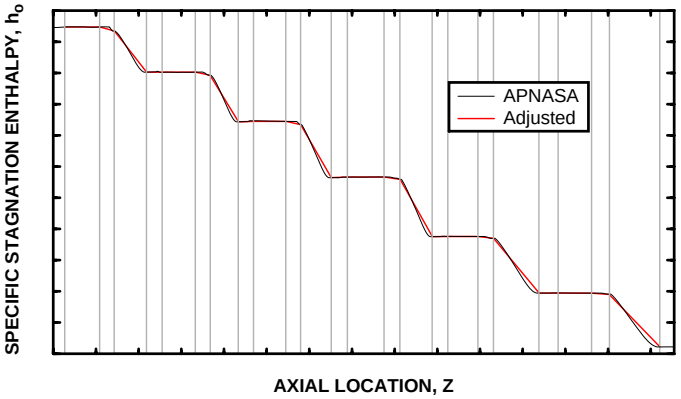

Figure 12. Comparison of converged APNASA and Adjusted LPT specific stagnation enthalpy as a function of axial location. Nozzle and rotor leading and trailing edges are indicated by vertical dashed lines.

enthalpy is shown in Fig. 12. As expected, there is very good agreement across the adiabatic nozzles, where stagnation enthalpy does not change. Across each nozzle-rotor and rotor-nozzle gap there is some divergence between the two curves as the adjusted data is unrealistically assumed to change only linearly. The data also shows very good agreement at the nozzle and rotor leading edges. The stagnation enthalpy is constrained to be identical at nozzle and rotor trailing edges. Comparison of APNASA and adjusted (rV_θ) data across the LPT showed similar agreement and is not presented here.

Entropy loss coefficient, ζ_s, for the LPT were computed by the *TurbinePreProcessor* for each individual bladerow and used in the on- and off-design simulations. For comparison purposes, the ζ_s data (see Table 6) is presented in GapA+Rotor, and GapB+Nozzle combinations to be consistent with the methodology used to match the APNASA CFD data; i.e., matching data at the Nozzle and Rotor trailing edges. The entropy loss coefficients are normalized by the Gap1A+Rotor1 value. Variations in the magnitude of ζ_s, are due mainly to the reaction and stage loadings chosen for this design.

Partial performance maps (i.e., mini-maps) for the HPT and LPT were generated by simulating each of the 1D turbine models over a small operating range. The speed was varied in 1 percent intervals from 98 to 102 percent of design speed for the HPT, and from 95 to 100 percent of design speed for the LPT. In both cases, the entropy loss coefficients for each bladerow were held constant.

The HPT and LPT mini-maps, shown in Figs. 13 and 14, plot pressure ratio and adiabatic efficiency as a function of corrected flow times corrected speed for the set of speed curves. Due to the proprietary nature of the GE90 data, the values of the plotted data cannot be shown. A comparison with GE cycle data showed that the HPT efficiency is 1.79 percent high, while the LPT is low by 1.54 percent [3]. A comparison of the APNASA solutions to rig data showed a similar trend for flow as reported by Turner *et al.* [9], with the HPT 2.5% high and the LPT 2.5% low relative to rig data. These differences are attributable to CFD modeling discrepancies such as the assumption of turbulent flow everywhere in the turbine. This is probably not the case for part of the LPT, and is probably why the LPT efficiency is low in the cycle with mini-maps. Another issue is that the loss models are incomplete in the 1D blade row models.

The solid triangles in Figs. 13 and 14 indicate the computed 1D design point corresponding to the sea-level, Mach 0.25, take-off condition. Note that, at the design point, both the HPT and LPT operate un-choked. The 1D turbine code is currently designed for un-choked flow; onset of choked flow is determined by increasing the mass flow rate until the code generates unrealistic values (these points are not plotted in the figures). As can be seen from both plots, the speed curves tend towards vertical as the pressure ratio increases, indicating choked flow.

Table 6: Normalized design point entropy loss coefficient, ζ_s, for LPT bladerow elements.

Element(s)	ζ_s
Nozzle 1	0.376523
Gap1A + Rotor1	1.000000
Gap1B + Nozzle2	0.342399
Gap2A + Rotor2	0.921279
Gap2B + Nozzle3	0.364855
Gap3A + Rotor3	1.177577
Gap3B + Nozzle4	0.390129
Gap4A + Rotor4	0.829845
Gap4B + Nozzle5	0.396952
Gap5A + Rotor5	0.375197
Gap5B + Nozzle6	0.384393
Gap6A + Rotor6	0.300443

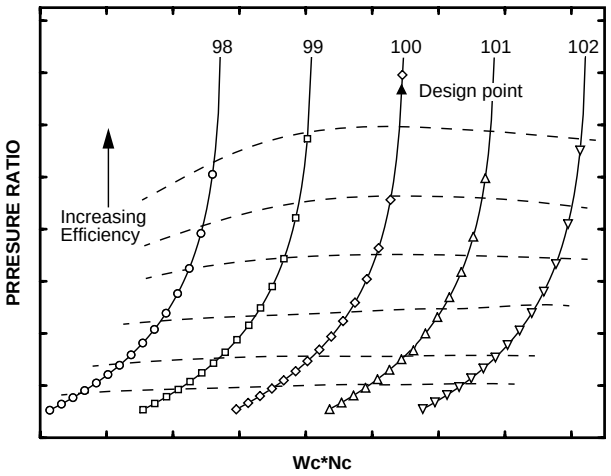

Figure 13. GE90 HPT mini-map depicting adiabatic efficiency (dashed lines) and pressure ratio as a function of corrected speed*corrected mass flow rate for a set of speed lines.

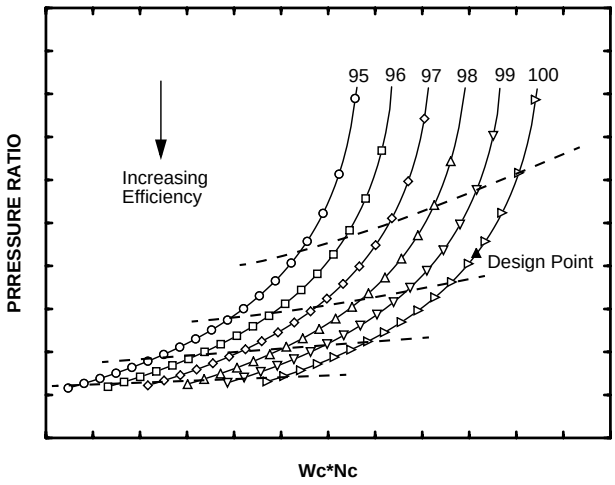

Figure 14. GE90 LPT mini-map depicting adiabatic efficiency (dashed lines) and pressure ratio as a function of corrected speed*corrected mass flow rate for a set of speed lines.

CONCLUSIONS

A new one-dimensional meanline bladerow model employing entropy-based loss terms, and including leakage and cooling flows, has been developed. Validation of the model and approach has been made using the GE EEE test data. A data match has been made at the design point and off-design simulations have been made by freezing the loss coefficients. The comparisons are good and demonstrate the appropriateness of the model for use in developing a mini-map.

A 3D APNASA CFD simulation of the combined GE90-94B HPT and LPT components was post-processed to provide leakage and averaged bladerow data, which was further processed to produce input data for 1D HPT and LPT models. Partial turbine performance maps (mini-maps) were then generated by simulating the models over a small operating range around the GE90-94B take-off point.

The research illustrates the utility of such a 1D model to represent the main and secondary flows in both shrouded and un-shrouded turbines. The use of entropy as a measure of loss is convenient as its value does not depend on whether it is viewed from relative or stationary frames. Furthermore, once the entropy of the fluid is known, only one other thermodynamic property is needed to determine the state of the fluid. Both aspects greatly simplify the numerical implementation of turbomachinery models.

While the comparison of GE90-94B efficiency maps is presented only qualitatively, the results are reasonable, despite the deficiencies of our loss model. Assuming total loss to be due to mixing and gross aerodynamics is appropriate: mixing is one of the largest contributors to loss in a shrouded turbine [10]. The Δs_{aero} loss term attempts to capture the other major loss mechanisms such as endwall and profile losses. The Δs_{aero} loss term predicts loss proportionally to the square of the velocity. Since we assume that ζ_s remains constant, the predicted loss is only reasonable within the small operating range around which the map was generated. For off-design operation, the model is incomplete as it does not specifically address incidence deviation, Mach number, loading, clearance and Reynolds number effects. Flow angles from the averaged CFD data are absolute air angles; currently no metal angles are provided with which to estimate incidence or deviation. In addition, there are small errors in the Δs_{mix} term due to the assumption of constant stagnation pressure mixing. This was done for convenience as the NPSS system performs constant pressure mixing by default.

The flow inside the hub and tip seals of a shrouded turbine is complex with interacting seal leakage jets and vortex flow structures [10]. Since the stagnation temperature and mass flow rate at the seal exits were known from the CFD data, we did not require a complicated model to accurately predict the seal exit conditions. However, our assumption that at off-design the seal loss varies proportionally to the square of the shaft speed is only a first-order approximation. A more sophisticated seal model would likely improve the simulation results. Most seal models (e.g., [1]), however, require the gap area, and flow angles to be known. In the present work a different approach was necessary because the APNASA model used sink and source terms to represent the seal leakage flow, and these data were not readily available from the CFD solution. An improved CFD or APNASA model should also be implemented and made consistent with this new 1-D model.

One of the critical issues when coupling models using different numerical methods or having different levels of fidelity is consistency. In the present work, which combined models at different spatial resolution (i.e, 1D and 3D), the averaging of the CFD solution resulted in flow parameters which were not identically conserved. Given the complexity of the turbomachinery model and the approximate nature of CFD, it is not sensible to expect the solution to converge to zero error. As a result, other methods must be developed. The approaches

presented here were satisfactory in this specific case and would be expected to be so in similar coupled turbomachinery simulations.

Another potential issue when coupling two numerical codes is discrepancies between the thermodynamic properties used to predict the flow state. In the present work, both NPSS and APNASA implement their own thermodynamic relationships. NPSS provides a mechanism for "pluggable" thermodynamic packages; that is, the thermodynamic routines used by NPSS elements can be changed at run-time. Available packages include CEA [11], JANAF [12], among others. This provides great flexibility when matching the thermodynamics used with a coupled code. However, in this case, there was no available package to match APNASA thermodynamics.

A third consistency issue we encountered was structural differences between models. This refers to ensuring that common physical structures are represented in both models. A typical example of this is the placement of bleeds. When matching the 1D model to a cycle model of the GE90-94B [2], we found it necessary to separate the nozzle 1 blade row from the 0D HPT element so that the nozzle 1 cooling flow would match the 1D model. Clearly this issue is highly dependent on the design and flexibility of the models used.

The simulation strategy presented in this paper is simple and flexible. Our approach is based only on conservation laws and a control volume approach. Loss coefficients have been determined without examining the details of the flow processes in the control volumes, and off design performance computed from a single CFD solution point. Although this simulation has been performed using the APNASA turbomachinery code, the approach is applicable to other CFD codes. Results from another CFD solution could be included in the 1D model by simply changing the *PreProcessorGenerator.*

Further work on the 1D model can focus on improving the seal and loss models, and extending the operation to handle choked flow. This approach can also be applied to other turbomachinery simulations, such as for compressors and fans.

ACKNOWLEDGMENTS

This work was supported by the NASA Ultra-Efficient Engine Technology (UEET) and NASA Aerospace Propulsion and Power programs. The authors would like to thank John Lytle, Joe Veres, Tom Lavelle, Brett Naylor, Greg Follen, and Scott Townsend at the NASA Glenn Research Center for their help in this effort. Special thanks to Larry Timko and Ron Plybon at General Electric for their assistance.

REFERENCES

[1] Denton, J. D., 1993, "Loss Mechanisms in Turbomachines," ASME *J. of Turbomachinery*, **115**, pp. 621-656.

[2] Reed. J. A., Turner, M. G., Norris, A., Veres, J. P., 2003, "Towards an Automated Full-Turbofan Engine Numerical Simulation," ISABE Paper No. 2003-1235.

[3] Turner, M. G, Reed. J. A., Ryder, R., and Veres, J. P., 2004, "Multi-Fidelity Simulation of a Turbofan Engine with Results Zoomed into Mini-Maps for a Zero-D Cycle Simulation," ASME Paper No. GT-2004-53956, *ASME Turbo Expo 2004 Power for Land, Sea, and Air*, June 14-17, 2004, Vienna, Austria.

[4] Lytle, J. K., 2000, "The Numerical Propulsion System Simulation: An Overview," NASA/TM-2000-209915.

[5] Lytle, J. K., 1994, "The Numerical Propulsion System Simulation: A Multidisciplinary design System For Aerospace Vehicles," NASA/TM-1999-209194.

[6] Lyman, F. A., 1993, "On the Conservation of Rothalpy in Turbomachines," *J. of Turbomachinery*, **115**, pp. 520-526.

[7] Halila, E.E, Lenahan, D.T, and Thomas, T.T, 1982, "High Pressure Turbine Test Hardware Detailed Design Report," NASA CR-167355.

[8] Timko, L.P., 1984, "Energy Efficient Engine High Pressure Turbine Component Test Performance Report," NASA CR-168289.

[9] Turner, M. G., Norris, A, Veres, J.P., "High Fidelity 3D Simulation of the GE90," AIAA Paper No. 2003-3996, June 2003, Orlando, FL.

[10] Grier, J., Stubert, B, Brouillet, B, and de Vito, L., 2003, "Interaction of Shroud Leakage Flow and Main Flow in a Three-Stage LP Turbine," ASME Paper No. GT-2003-38025, *ASME Turbo Expo 2003*, June 16-19, 2003, Atlanta, USA.

[11] McBride, B. J, Zehe, M. J., Gordon, S., 2002, "NASA Glenn Coefficients for Calculating Thermodynamic Properties of Individual Species," NASA/TP-2002-21156.

[12] JANAF Thermochemical Tables, 3rd edition, M.W. Chase Jr., C.A. Davies, J.R. Davies, Jr., D.J. Fulrip, R.A. McDonald, and A.N. Syverud, *Journal of Physical and Chemical Reference Data*, **14**, Supplement 1, 1985.